IEEE Access
Multidisciplinary | Rapid Review | Open Access Journal

Received 3 July 2022, accepted 15 July 2022, date of publication 20 July 2022, date of current version 25 July 2022.

Digital Object Identifier 10.1109/ACCESS.2022.3192548

RESEARCH ARTICLE

Design Methodology of Multiband Printed Antennas for Future Generations of Mobile Handsets

ASMAA E. FARAHAT, KHALID F. A. HUSSEIN, AND MAY ABO. EL-HASSAN
Microwave Engineering Department, Electronics Research Institute, Cairo 11843, Egypt
Corresponding author: Khalid F. A. Hussein (fkhalid@eri.sci.eg)

ABSTRACT The present paper introduces a design methodology to extend the operation of a microstrip patch antenna to operate efficiently at multiple higher-order resonances. This method depends on the geometrical modification of the antenna structure by adding well-designed inductively-loaded and capacitively-coupled elements to the primary patch so that it can efficiently radiate at the desired higher frequency bands. It is explained quantitatively how to use the geometrical parameters of the inductively and capacitively coupled elements for accurate tuning of the multiple resonant frequencies of the antenna. The proposed method is applied to modify a primary hexagonal patch antenna (designed to principally radiate at 28 GHz as its first-order resonance) so as to operate at additional higher frequency bands around 43, 52, and 57 GHz. Also, an alternative design is provided for a quad-band printed antenna of composite patch structure that operates in the same millimetric-wave (mm-wave) bands, 28, 43, 52, and 57 GHz with high radiation efficiency, excellent impedance matching, and satisfactory values of the antenna gain. The corresponding frequency bands are, respectively, (27.7-28.3 GHz), (42.7-43.3 GHz), (51.2-53.0 GHz), and (55.7-57.5 GHz). The dimensions of the area occupied by the primary patch and the parasitic elements are 5.2×3.3 mm^2. The two antennas are fabricated for experimental assessment of their performance including the impedance matching and radiation patterns. It is shown that the experimental measurements come in agreement with the simulation results over all the four operational mm-wave frequency bands. One of the advantages of the proposed method is that it can be applied to patch antennas of arbitrary shapes and is not restricted to hexagonal patch antennas. Furthermore, this method is not restricted by extending the operation of the antenna to radiate at four frequency bands. It is capable of adding any desired number of frequency bands so that the antenna can operate at five or, even, more bands.

INDEX TERMS MIMO, multi-band antenna, patch antenna, 5G mobile communications.

I. INTRODUCTION

One of the essential demands for the future generations of mobile communications is the capability of the mobile handsets to transfer data with very high speed. A mobile handset antenna should have compact profile and simple structure [1], [2]. To meet the standards of long-term-evolution (LTE) and fifth generation (5G) of mobile communications [3] an antenna of handheld device should provide broadband operation, high data rate and low power consumption. This recommends that a mobile handset antenna should be able to operate in the range of mm-wave of the electromagnetic spectrum to support the required data rates for the future applications. Moreover, due to size limitations, it is recommended that a mobile handset antenna is able to operate efficiently at multiple frequency bands in the mm-wave spectrum to support the applications of the forthcoming mobile generations [4], [5].

The antenna structure may be complicated as those having three-dimensional shape to operate efficiently in a single frequency band and to perform some function in special applications [6], [7] and may include layers with high

The associate editor coordinating the review of this manuscript and approving it for publication was Ravi Kumar Gangwar.

electromagnetic absorbance [8] to produce radiation patterns of desired shape. However, for mobile handsets, due to size and weight limitations, it is preferable to have planar antenna of simple-structure, multi-band operation and omnidirectional radiation patterns.

Single-element antennas as well as MIMO antenna systems for 5G mobile handsets, recently, have been designed in a lot of research articles. The work of [9] introduces a dual-band mm-wave circular microstrip patch antenna with an elliptical slot. A dual-band (38/54GHz) microstrip antenna designed for 5G mobile communications is presented in [10]. EBG reflector is integrated into the MIMO antenna system to operate at Ka-band is introduced in [11]. The work of [12] presents a patch antenna with parasitic elements in the same layer to improve its bandwidth. Also, dual-band 28/38 GHz high-gain antennas are presented in [13], and [14]. In [15], a quad-band (28/45/51/56 GHz) antenna is proposed for the 5G mobile communication system.

Several techniques have been proposed to modify a single-band patch antenna to have multiband operation. For example, in [16], a coplanar waveguide (CPW) feed technique is introduced where two coupled radiating elements composed of rectangular ring microstrip and a folded meandered are fed by 50Ω CPW to design a four-band patch antenna. A fractal technique is proposed in [17] to design a five band microstrip-line-fed modified star triangular patch antenna. In [18], multiband microstrip patch antenna is designed using nature-inspired optimization method with three slits for some frequency bands of cellular communication networks. Another technique based on the mechanism of proximity coupled feeding is introduced in [19] where a corner-truncated rectangular patch with a rectangular slot on a defected ground plane is fed through a meandered microstrip line. Another technique employing inverted-L- and T-shaped parasitic elements placed at both the radiating apertures of a microstrip patch antenna with three operational frequency bands is proposed in [20].

The present work introduces a novel method to extend the operation of a microstrip patch antenna that is designed to principally radiate at 28 GHz as its first-order resonance so that it can efficiently operate at additional multiple higher frequency bands around 43, 52.5, and 57 GHz. In spite of being applied to modify the design of a hexagonal patch antenna, the method proposed in the present work can be applied to patch antennas of various shapes. This method depends on the geometrical modification of the antenna structure by adding some inductively and capacitively coupled elements to the primary hexagonal patch so that it can efficiently radiate at some desired higher frequency bands. The present work provides quantitative explanation of how the geometrical parameters of the inductively and capacitively coupled elements can be used for accurate tuning of the multiple higher-order resonant frequencies of the antenna.

The present paper is organized as follows. Section II provides a description of a hexagonal patch antenna that is designed to principally radiate at 28 GHz. Section III gives detailed explanation of the multiband design methodology that depends on the geometrical modification of the antenna structure by adding some inductively and capacitively coupled elements to the primary patch so that it can radiate at the desired higher frequency bands. Section IV provides another example of quad-band antenna that operates at 28, 43, 52, and 57 GHz. Section V provides numerical simulation and experimental assessment of the of the quad-band antennas performance. Section VI gives a summary of the most important conclusions of the present work.

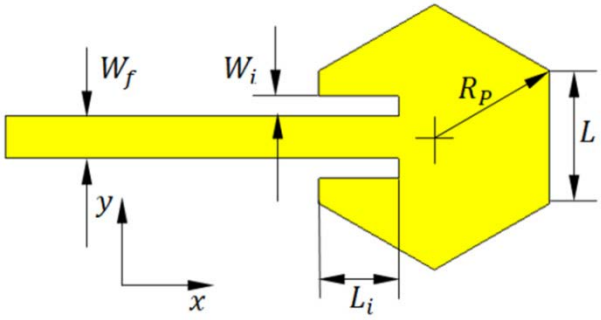

FIGURE 1. Hexagonal patch designed to principally radiate at 28 GHz.

II. DESIGN OF HEXAGONAL PATCH ANTENNA TO PRINCIPALLY RADIATE AT 28 GHZ

The Rogers RO3003 substrate of $\epsilon_r = 3.0$ and height, $h = 0.25$ mm is used for the proposed hexagonal patch antenna. Using such a substrate on a solid ground structure (without any defects), a hexagonal patch antenna with inset feed as that shown in Fig. 1 can be designed by setting its dimensional parameters to operate at the desired frequency.

Like a circular patch antenna, the radius of the hexagonal patch, R_p, determines the frequency at which the first order mode is excited in the cavity below the patch. It can be approximated as follows [21], [22],

$$R_P = F\left\{1+\frac{2h}{\pi\epsilon_r F}\left[\ln\left(\frac{\pi F}{2h}\right)+1.7726\right]\right\}^{-1/2},$$
$$F = \frac{8.791\times10^7}{f_0\sqrt{\epsilon_r}} \quad (1)$$

The width of the feeding microstrip line is set to realize characteristic impedance $Z_o = 50\Omega$ using the rules supplied in [22] for this purpose. The inset length is determined so as to match the patch impedance to the 50Ω microstrip line feeder using the following formula [21].

$$L_i = 10^{-4}R_P\sum_{n=0}^{7}a_0\epsilon_r^n \quad (2)$$

It is required to set the dimensional parameters to the proper values so as to get the hexagonal patch antenna principally operational at 28 GHz. These dimensional parameters are the side length, L, of the hexagonal patch (equivalently, the patch radius R_P), the inset length, L_i, and the width of the

TABLE 1. Dimensional parameters of the antenna structure shown in Fig. 1.

Dimension	R_P	L_i	W_i	W_f
Value (mm)	1.99	1.18	0.3	0.63

slots, W_i, which are cut on the sides of the feeding line for inset feed. It should be noted that the expressions (1) and (2) are just used to give initial estimates for the patch radius R_P, and inset length, L_i, however, the selection of the best values for these parameters is to be performed through extensive parametric study as explained in the next subsection. The mechanism of radiation of the hexagonal patch antenna presented in Fig. 1 depends on the excitation of the first order cavity mode at the desired operational frequency of the antenna. In a manner similar to the circular patch antenna, the hexagonal patch is fed to excite the TM_{11} mode in the cavity below the patch. The patch radiates through the slots surrounding the cavity between the patch and the ground plane. The optimum values of the dimensional parameters of the antenna presented in Fig. 1 are listed in table 1. These optimum values of the dimensional parameters are obtained through an extensive parametric study explained in the following subsections.

The hexagonal patch is selected as a primary patch for the proposed antenna owing to its first four resonant frequencies 28, 45, 50, and 55 GHz that are distributed over the mm-wave range 28-55 GHz as shown later in the present work. Simple modification of such patch geometry can be made to slightly change the locations of the resonant frequencies so as to get them close to the desired operational frequencies.

An equivalent circuit model of the hexagonal patch antenna can be deduced using the transmission line model in a way similar to that followed in [23], and [24]. The patch circuit model is shown in Fig. 2. The cavity subtended between the hexagonal patch and the ground plane can be modeled using the three elements R_a, L_a, C_a as shown in Fig. 2. The patch resonance is calculated as follows.

$$f_0 = \frac{1}{2\pi\sqrt{L_a C_a}} \tag{3}$$

At this frequency, the reactance of L_a cancels that of C_a. The series inductance L_s is added to the circuit model to account for the non-zero thickness of the patch. Thus, at resonance, the input impedance of the patch can be expressed as follows.

$$Z_{\text{in}} = R_a + j2\pi f_0 L_s \tag{4}$$

In the equivalent circuit model, the conductances, G_1 and G_2 account for the power loss due to radiation from the first and second radiating slots, respectively. The susceptances B_1 and B_2 account for the reactive power storage in the cavity surrounded by the radiating slots.

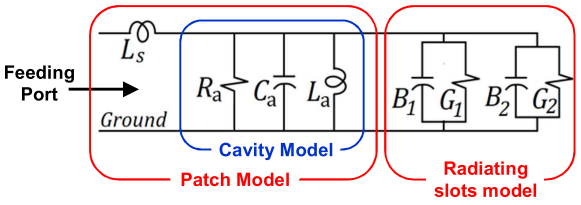

FIGURE 2. Equivalent circuit of the inset-fed hexagonal patch presented in Fig. 1.

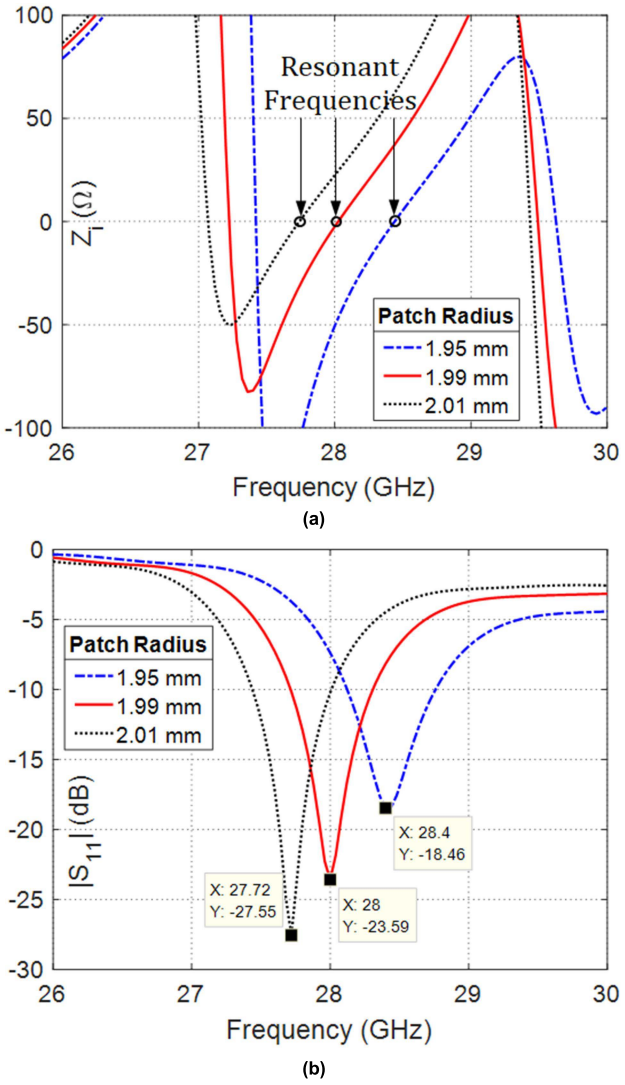

FIGURE 3. Frequency dependece of (a) the reactive part of the antenna input impedance and (b) the corresponding reflection coeficient, $|S_{11}|$, over a wide frequency range around 28 GHz for different values of the patch radius, R_P.

A. PARAMETRIC STUDY OF THE HEXAGONAL PATCH ANTENNA FOR OPTIMUM PERFORMANCE AT 28 GHZ

For optimum design of the hexagonal patch antenna at 28 GHz, the effects of the dimensional parameters R_P, L_i, and W_i, are numerically studied. The patch radius, R_P, is mainly responsible for identifying the resonant frequency of the

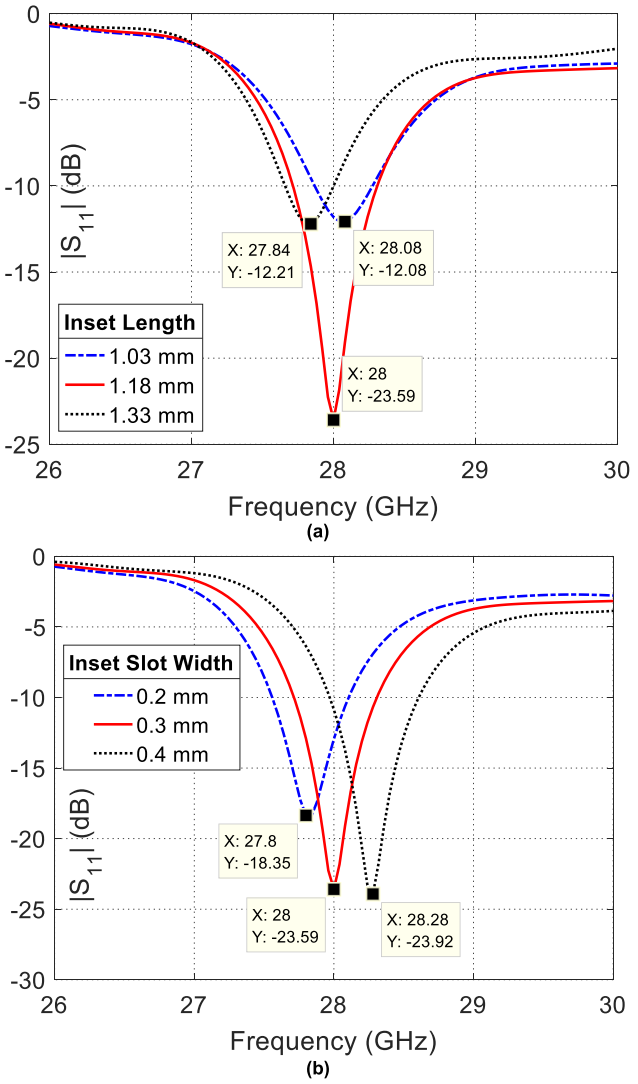

FIGURE 4. Frequency dependence of the reflection coefficient, $|S_{11}|$, over a wide frequency range around 28 GHz for different values of (a) the inset length, L_i, and (b) the inset slot width W_i.

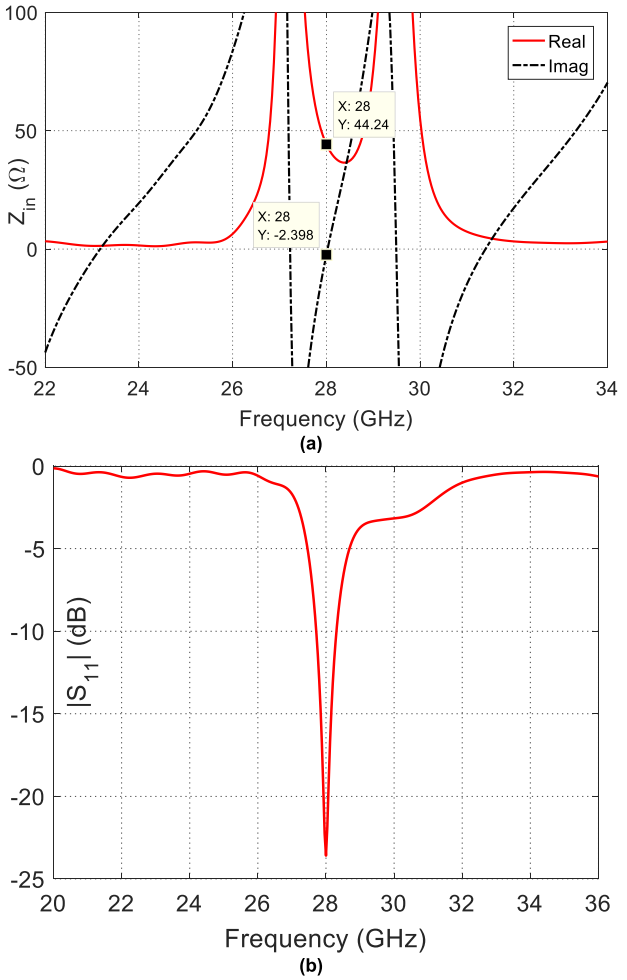

FIGURE 5. Frequency dependece of (a) the antenna input impedance and (b) the corresponding reflection coeficient, $|S_{11}|$, showing a resonance with excellent impedance matching at 28 GHz.

patch. As shown in Fig. 3a, the resonant frequency (at which the imaginary part of the patch impedance vanishes) is inversely proportional to R_P. Also, it is shown in Fig. 3b that the best impedance matching at 28 GHz is obtained when $R_P = 1.99$ mm. The minimum value of $|S_{11}|$ is obtained when the inset length $L_i = 1.18$ mm as shown in Fig. 4a. On the other hand, the effect of the width of the slots, W_i, which are cut on the sides of the feed line, on the reflection coefficient $|S_{11}|$ is presented in Fig. 4b. It is shown that setting $W_i = 0.3$ mm gives the minimum value of $|S_{11}|$ exactly at 28 GHz.

B. FINAL DESIGN OF THE HEXAGONAL PATCH AT 28 GHz

The frequency dependence of the real and imaginary parts of the antenna input impedance over a frequency range around 28 GHz is presented in Fig. 5a. It is shown that the patch has a resonance at 28 GHz. At this frequency, the imaginary part of the antenna impedance is very close to zero (-2.4Ω) whereas the real part is about 44.2Ω. Therefore, when the antenna is fed by a line of 50Ω characteristic impedance, the frequency dependence of the reflection coefficient, $|S_{11}|$, shows excellent impedance matching at 28 GHz as shown in Fig. 5b. The width of the microstrip line used for feeding the antenna is set as $W_F = 0.63$ mm to get its characteristic impedance equal to 50Ω.

The radiation patterns produced at 28 GHz by such a hexagonal patch antenna with the dimensional parameters, $L = 1.99$ mm, $L_i = 1.18$ mm, and $W_i = 0.3$ mm, in the elevation planes $\phi = 0°$ and $\phi = 90°$, are presented in Fig. 6a. It is shown that the radiation patterns in the two orthogonal elevation planes are almost identical, which indicates circularly-symmetric radiation pattern in the azimuth planes as shown in Fig. 6b. The maximum gain of the antenna is about 7 dBi in the direction $\theta = 0$ (z-direction).

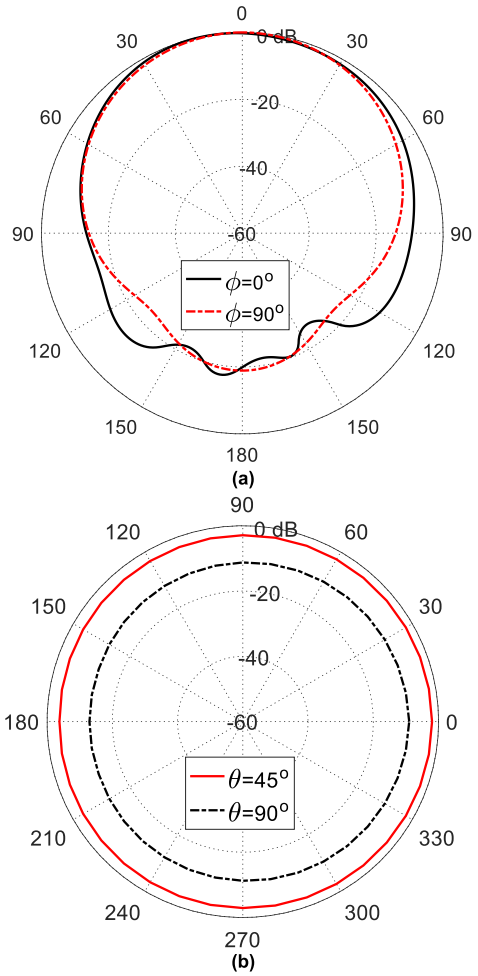

FIGURE 6. Radiation patterns of a hexagonal patch antenna at 28 GHz (a) in the elevation planes $\phi = 0°$, and $\phi = 90°$, and (b) in the azimuth planes $\theta = 45°$, and $\theta = 90°$.

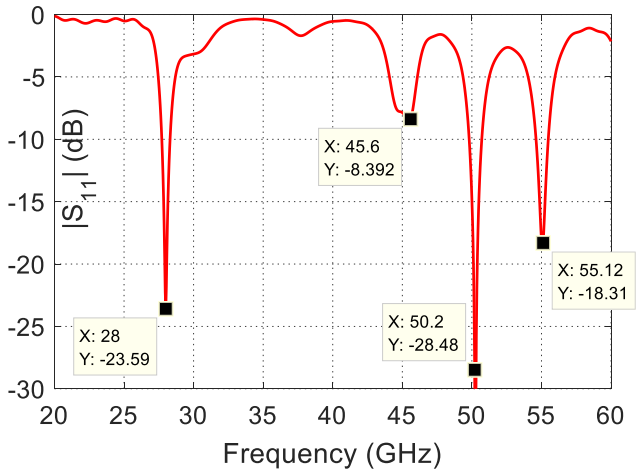

FIGURE 7. Frequency dependence of the reflection coefficient $|S_{11}|$ at the feeding port of the hexagonal patch antenna shown in Fig. 1.

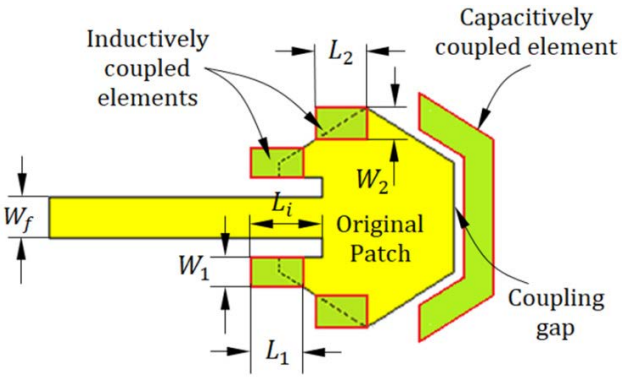

FIGURE 8. Examples of various types of secondary patch elements that can be added to the antenna structure as inductive or capacitive loads.

III. MODIFICATION OF THE HEXAGONAL PATCH ANTENNA TO EFFICIENTLY RADIATE AT HIGHER FREQUENCIES

A novel method is introduced in the present work to improve the performance of the primary patch antenna, introduced in Section II, so as to properly operate at the desired higher order resonances. This method depends on modifying the antenna input impedance so as to get it resonant, i.e. to eliminate the imaginary part of its input impedance at the desired frequency and to get the real part of the impedance as close as possible to the 50Ω.

The hexagonal patch antenna whose design is presented in Fig. 1 has the frequency dependence of the reflection coefficient $|S_{11}|$ shown in Fig. 7 over the frequency range 20-60 GHz. It is clear that this patch has its first four resonances at the frequencies 28, 45, 50, and 55 GHz. It is shown that value of $|S_{11}|$ at some resonances is not below -20 dB. In the present section, a method is described to control the locations of the higher-order resonant frequencies and to improve the corresponding impedance matching (assuming 50Ω source). The method proposed in the present work depends on the addition of secondary patch elements to the original hexagonal patch.

To get the hexagonal patch antenna efficiently operational at multiple higher-order frequencies, reactive loads can be added to the basic hexagonal patch antenna. It is suggested to modify the geometry of the hexagonal patch by adding metallic parts to the patch as shown in Fig. 8, where the suggested additional parts are presented in green color. Two types of such loads can be used to control the locations of the resonant frequencies and to improve the impedance matching at these frequencies: inductively-loaded and capacitively-loaded elements. The equivalent circuit model of the modified patch antenna is presented in Fig. 9. The rectangular patches overlapped with the hexagonal patch can be seen as inductively-coupled (short-circuited) to the main patch. The inductively-loaded elements can be represented by shunt coil and resistance (conductance G_c) as shown in the circuit model. On the other hand, the inverted C-shaped parasitic patch can be seen as capacitively coupled (open-circuited) to the main patch. Such capacitively-loaded element can be represented by shunt capacitance (suseptance B_p) and resistance

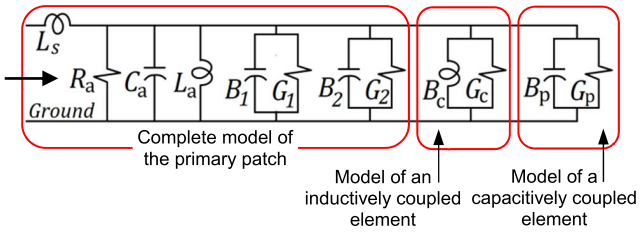

FIGURE 9. Equivalent circuit of the inset-fed hexagonal patch when loaded by inductively and capacitively coupled elements as presented in Fig. 8.

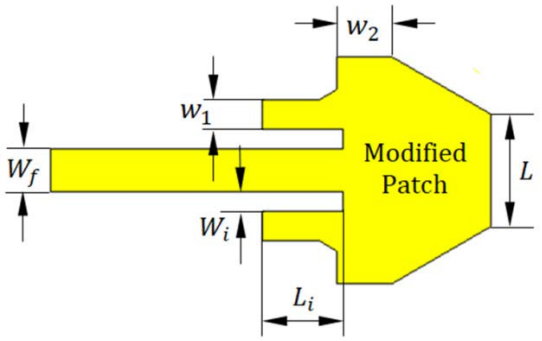

FIGURE 10. Patch antenna after welding the inductively loaded (short-circuited) secondary elements to the original hexagonal patch.

TABLE 2. Dimensional parameters of the antenna structure shown in Fig. 10.

Dimension	L	L_i	W_i	L_G	W_G	W_1	W_2	W_f
Value (mm)	1.99	1.18	0.3	2.06	0.28	0.45	0.85	0.63

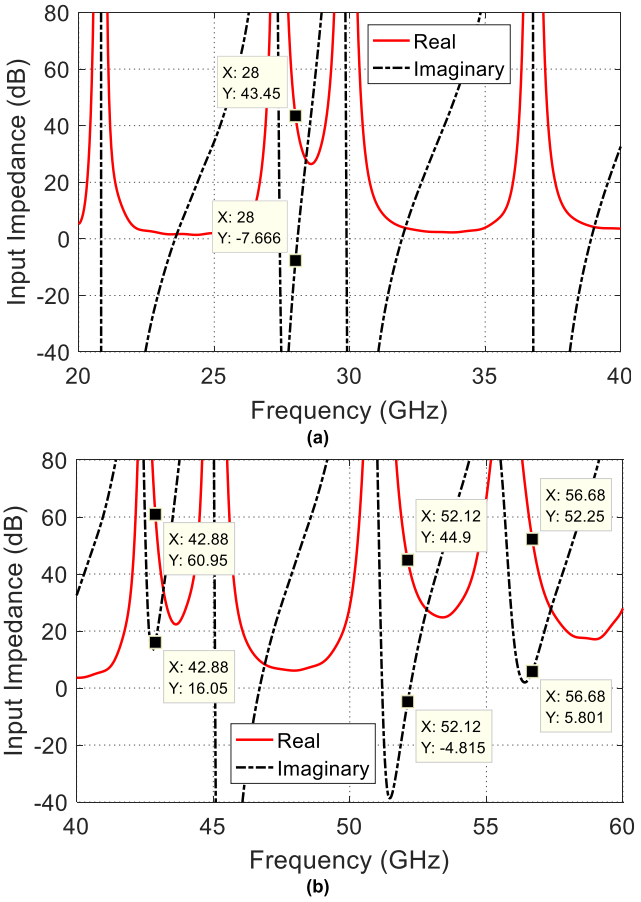

FIGURE 11. Frequency dependence of the input impedance of the modified patch antenna (shown in Fig. 8) in the frequency ranges (a) 20-40 GHz, and (b) 40-60 GHz.

(conductance G_p) as shown in the circuit model. Both types of loads can be used for tuning the resonant frequencies and, in the meantime, to control the antenna impedance at these resonances.

A. LOADING THE MAIN PATCH BY INDUCTIVELY-COUPLED ELEMENTS

Merging the inductively loaded (short-circuited) secondary elements to the original hexagonal patch, results in the modified patch shown in Fig. 10. The modified patch has the frequency dependence of its input impedance as shown in Fig. 11. It is clear that the antenna has five resonances at which the imaginary part of its impedance vanishes whereas the real part is close to 50Ω and, hence, the modified antenna can be considered of good impedance matching at the four frequencies 28, 42.88, 52.12, and 56.68 GHz. This can be shown in Fig. 12 where the magnitudes of the reflection coefficient are very low at the four frequencies. The dimensional parameters of the antenna structure shown in Fig. 10 are listed in table 2.

When compared to the frequency response of the reflection coefficient shown in Fig. 7, the frequency response of the modified patch, presented in Fig. 10 shows significant improvement of the antenna performance at the desired resonant frequencies. The inductively coupled elements cause the imaginary part of the antenna impedance to vanish at the desired frequencies whereas the corresponding real part is very close to 50Ω at these frequencies.

B. LOADING THE MAIN PATCH BY CAPACITIVELY-COUPLED SECONDARY ELEMENTS

For further improvement of the antenna performance and to get the final antenna structure operational at the multiple bands around 28, 43, 52.5, and 57 GHz, capacitively-coupled secondary patch elements can be added to the primary patch shown in Fig. 10. The geometrical shape, dimensions, and position of the parasitic element relative to the primary patch can be set to control the resonant frequencies of the multiple operational bands of the final antenna structure.

The secondary patch should be coupled to the primary patch through a well-designed gap i.e. of suitable shape, width and length. For example, an arc or inverted-C shaped parasitic patch can be capacitively loaded (edge coupled) to the primary patch as shown in Fig. 13. It should be noted

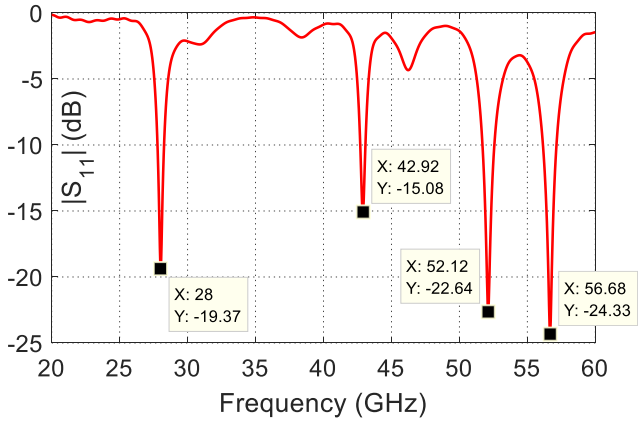

FIGURE 12. Dependence of the reflection coefficient $|S_{11}|$ of the modified patch antenna (presented in Fig. 10) on the frequency.

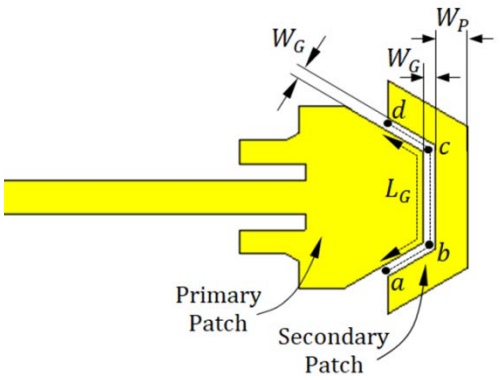

FIGURE 13. Proposed quad-band patch loaded by a secondary parasitic patch through capacitive edge coupling.

that the reactive coupling between the primary patch and the inverted-C shaped parasitic patch is strongly dependent on the gap dimensions between the two patches. The coupling gap width is given as W_G, whereas the coupling length L_G is equal to the length of the path *abcd* indicated in Fig. 13. The dimensional parameters of the antenna structure shown in Fig. 13 are listed in table 3. The frequency dependence of the reflection coefficient of the capacitively loaded patch is shown in Fig. 14.

It may be worthwhile to mention that the antenna presented in Fig. 13 has already been included in [25] with little differences. However, the design methodology (the core subject of the present work) is not presented in [25]. As mentioned earlier in the present paper, the main objective of the present work is to present the novel design methodology to realize the multiband operation of printed antennas for the forthcoming generation of mobile applications. Also, the present work involves elaborate presentations of theoretical and experimental assessment of the proposed methodology using more than one antenna design example including that presented in [25].

TABLE 3. Dimensional parameters of the antenna structure shown in Fig. 13.

Dimension	L	L_i	W_i	W_P	L_G	W_G	W_1	W_2	W_f
Value (mm)	1.99	1.18	0.3	0.8	2.06	0.28	0.45	0.85	0.63

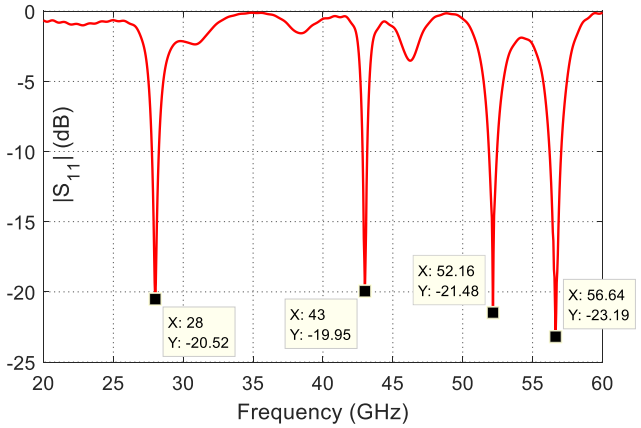

FIGURE 14. Dependence of the reflection coefficient $|S_{11}|$ of the modified patch antenna (presented in Fig. 11) on the frequency.

1) ROLE OF THE PARASITIC ELEMENTS

Definitely, the reactive load caused by the coupling between the primary and parasitic patches is strongly dependent on the geometry of the secondary patch and, also, on the width and length of the coupling gap. Consequently, some of the dimensional parameters can be set to get the antenna properly operating at some frequency bands whereas other dimensional parameters can be set to enhance the antenna performance at the other frequency bands. In the following, some examples are presented to explain how to get the antenna appropriate to operate at the multiple desired frequency bands. For example, the second frequency band, the antenna input impedance and, hence, the reflection coefficient relative to 50Ω source impedance is sensitive to the gap width, W_G, as shown in Fig. 15a. It is noticed that the other three operational bands (first, third, and fourth bands) seem to be insensitive to (almost unaffected by) the variations of W_G. Thus, for fine tuning of the central frequency of the second band without affecting the other operational bands, it is recommended to vary the gap width, W_G, within the range indicated in Fig. 15b. In this way, the center of this frequency band can be finely tuned.

Over the third operational frequency band (around 52 GHz), the antenna input impedance and, hence, the reflection coefficient are sensitive to the gap length, L_G when is varied from 2.06 mm to 2.22 mm, as shown in Fig. 16a. The other three operational bands (first, second, and fourth bands) seem to be almost unaffected by the variations of L_G within this range (2.06 − 2.22 mm). Thus, for fine tuning of the central frequency of the third band without affecting the other

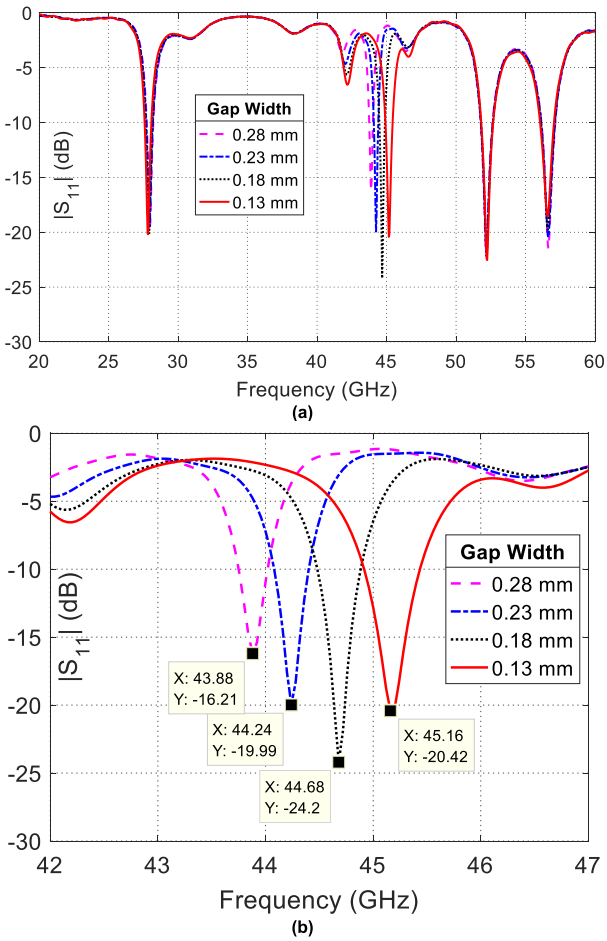

FIGURE 15. Dependence of the reflection coefficient $|S_{11}|$ on the frequency for different values of the gap width, W_G, (a) over the frequency range 20 – 60 GHz, (b) over the frequency range around the second operational band 42 – 47 GHz.

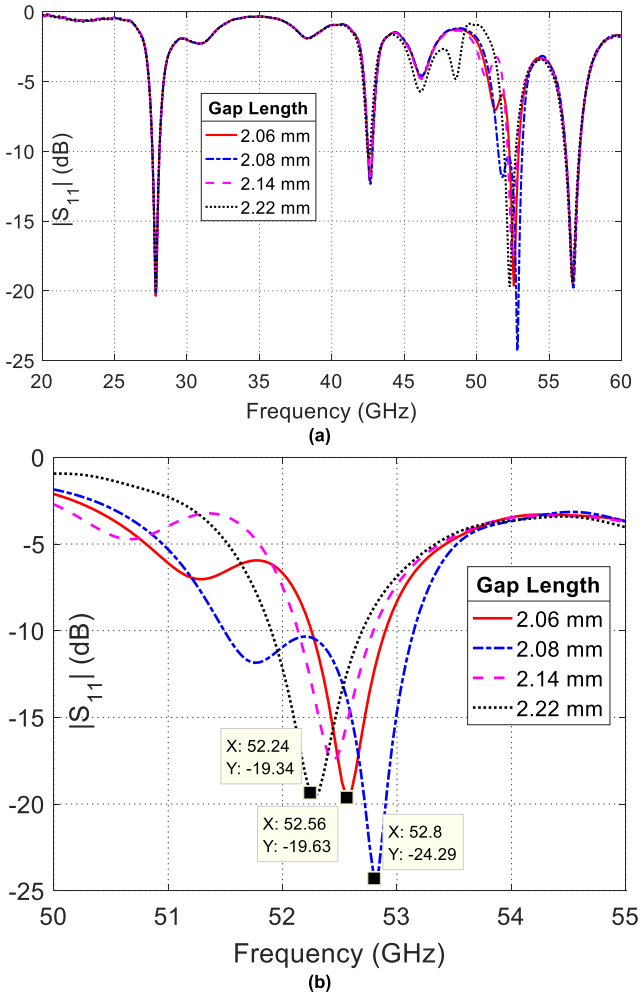

FIGURE 16. Dependence of the reflection coefficient $|S_{11}|$ on the frequency for different values of the gap length, L_G, (a) over the frequency range 20 – 60 GHz, (b) over the frequency range around the second operational band 50 – 55 GHz.

operational bands, it is recommended to vary the gap length within the range indicated in Fig. 16b. In this way, the central frequency of this band can be finely tuned.

The fourth operational frequency band is desired to be centered at 57 GHz, the antenna input impedance and, hence, the reflection coefficient is sensitive to the gap length, L_G, when varied in the range 1.90 mm to 2.06 mm, as shown in Fig. 17a. The other three operational bands (first, second, and third bands) seem to be insensitive to (almost unaffected by) the variations of L_G within this range (1.90 − 2.06 mm). Thus, for fine tuning of the central frequency of the fourth band without affecting the other operational bands, it is recommended to vary the gap length, L_G, within the range indicated in Fig. 17b. In this way, the fourth operational frequency band can be adjusted at 57 GHz as desired. Thus, setting the dimensional parameters $L_G = 2.06$ mm, satisfies the desired operational frequencies for the second and third frequency bands.

2) FABRICATION AND MEASUREMENTS

In this section, the simulation and experimental results obtained for the quad-band antenna shown in Fig. 13 with the dimensional parameters listed in Table 3 are presented and compared to each other to confirm the accuracy of the results concerned with the evaluation of the antenna performance assessment over the four operational frequency bands. The fabricated prototype is shown in Fig. 18a where it is connected to the coaxial end launcher.

The experimental setup for the measuring S_{11} using the VNA model ZVA67 is illustrated in Fig. 18b. The variation of $|S_{11}|$ with the frequency is shown in Fig. 19. It is shown that both the measured and simulated responses of $|S_{11}|$ with the frequency agree with each other to ensure that the proposed mm-wave patch perfect impedance matching at 28, 43, 52, and 57 GHz.

IV. ANOTHER DESIGN OF THE PRINTED ANTENNA FOR QUAD-BAND OPERATION

The same methodology described in the present work to construct multiple-band antenna structure starting with a hexagonal patch antenna (that is designed to principally radiate at 28 GHz) is applied, in the present section, to arrive at

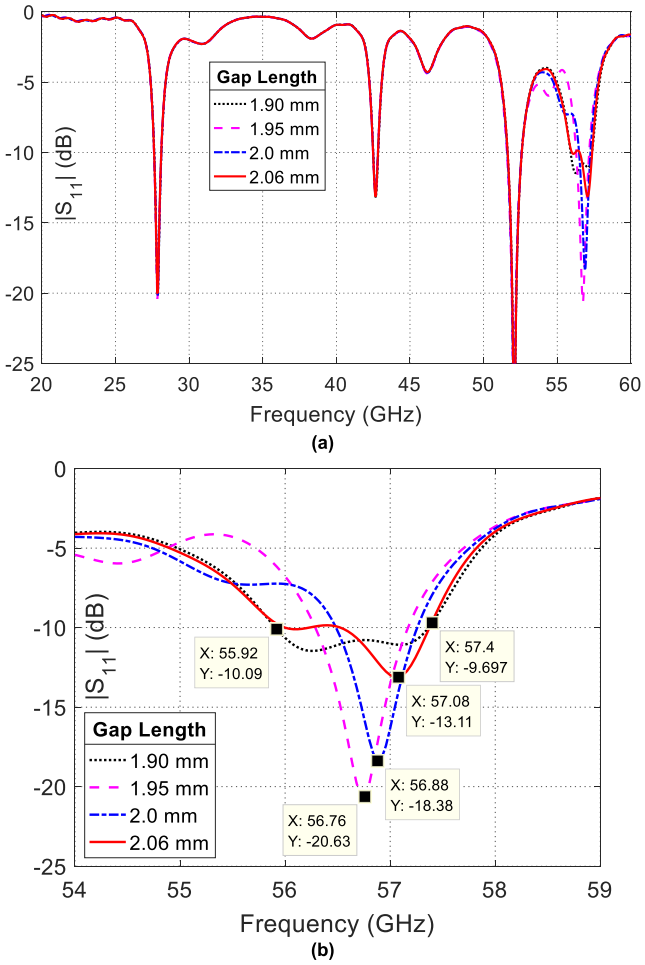

FIGURE 17. Dependence of the reflection coefficient $|S_{11}|$ on the frequency for different values of the gap length, L_G, (a) over the frequency range 20 – 60 GHz, (b) over the frequency range around the second operational band 54 – 59 GHz.

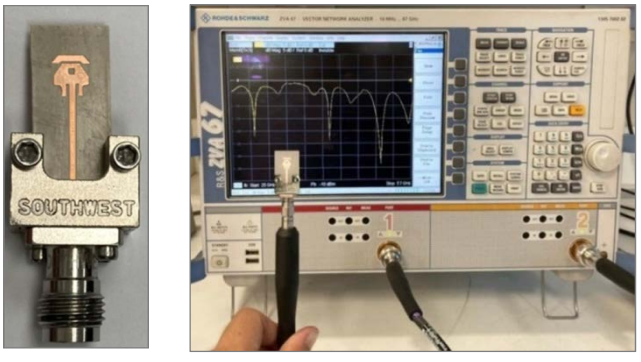

FIGURE 18. (a) Fabricated prototype of the quad-band patch antenna of the design presented in Fig. 13 connected to the end launcher (b) Experimental assessment of $|S_{11}|$ over the frequency range 20 – 60 GHz using the VNA.

the design of the quad-band printed antenna structure shown in Fig. 20. In addition to the inductively- and capacitively-coupled secondary elements that are added to the primary

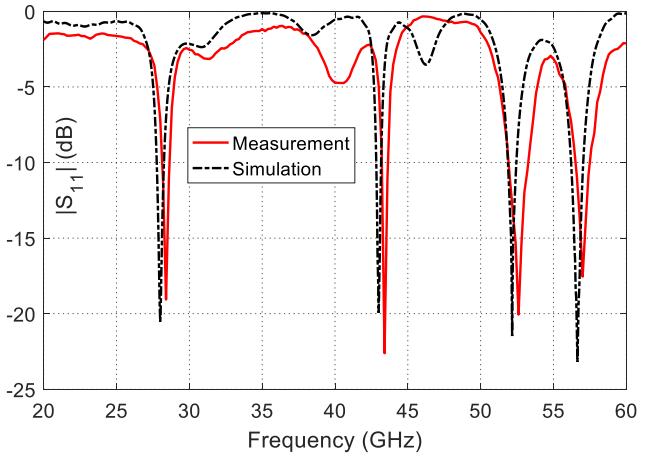

FIGURE 19. Comparison between the simulated and measured reflection coefficient $|S_{11}|$ over the frequency range (20-60) GHz for the quad-band patch antenna presented in Fig. 13.

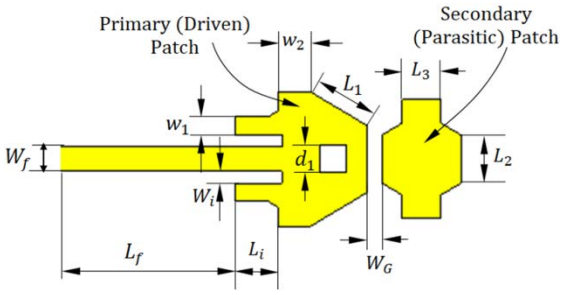

FIGURE 20. Geometry of quad-band composite patch antenna.

patch structure to improve the antenna performance, a rectangular cut is made in the primary patch at the location shown in Fig. 20 where the surface current on the patch is very weak and can be negligible. The values of the dimensional parameters of the new printed antenna design are listed in Table 4. For practical assessment of the quad-band antenna through experimental measurements, the antenna is fabricated on Rogers RO3003 substrate of dimensions $W \times L = 10 \times 18$ mm^2, thickness $h = 0.25$ mm, dielectric constant $\varepsilon_r = 3$, and loss tangent $\tan\delta = 0.001$. The dimensions of the feeding microstrip transmission line are $W_f \times L_f = 0.63 \times 10.03$ mm^2. An inset feed is used to match the antenna impedance to 50Ω source where $W_i \times L_i = 0.3 \times 1.23$ mm^2. The fabricated antenna is shown in Fig. 21 where its size is compared to the size of a standard one-inch metallic coin. This antenna operates efficiently over the four bands centered at 28, 43, 52, and 57 GHz.

V. NUMERICAL SIMULATION AND EXPERIMENTAL ASSESSMENT OF THE QUAD-BAND PATCH ANTENNA

In this section, the simulation and experimental results obtained for the proposed quad-band antenna are presented and compared to each other to confirm the accuracy of the results concerned with the evaluation of the antenna performance. The quad-band printed antenna whose design is

TABLE 4. Dimensional parameters of the antenna structure shown in Fig. 20.

Dimension	R_P	L_i	W_i	w_1	w_2
Value (mm)	1.99	1.23	0.3	0.45	0.85
Dimension	L_1	L_2	L_3	W_G	d_1
Value (mm)	1.7	1.2	1	0.38	0.7

FIGURE 21. Fabricated prototype of the proposed quad-band patch antenna with its size compared to a metal coin of standard size.

TABLE 5. List of the devices used for experimental measurements of the antenna input impedance and radiation characteristics.

Device	Model	Frequency Range
Vector Network Analyzer (VNA)	Rhode & Schwartz ZVA67	10 MHz – 67 GHz
Vector Signal Generator (VSG)	Agilent E8267D	100 KHz – 44 GHz
Vector Signal Analyzer (VSA)	Agilent N9010A	10 Hz – 44 GHz
Reference Horn Antenna (20dBi-Gain)	A-Info LB018400	18 – 40 GHz
Reference Horn Antenna (20dBi-Gain)	A-Info LB-12-10-A	40 – 60 GHz

shown in Fig. 20 with the dimensional parameters listed in Table 4 and whose fabricated prototype is shown in Fig. 21 is subjected to experimental assessment over the four operational frequency bands.

A. EXPERIMENTAL ASSESSMENT OF THE ANTENNA PERFORMANCE

The experimental assessment involves the evaluation of the antenna input impedance and the radiation patterns in the elevation planes. The equipment listed in Table 5 are used for this purpose. The 1.85 mm end-launch connector is used to connect the antenna prototype to the test equipment as shown in Fig. 22a.

The VNA is used to measure the antenna input impedance and, hence, the reflection coefficient S_{11} over the frequency range 20 – 60 GHz. The VSG-E8267D and VSA-N9010A are used to measure the radiation patterns at 28 GHz using

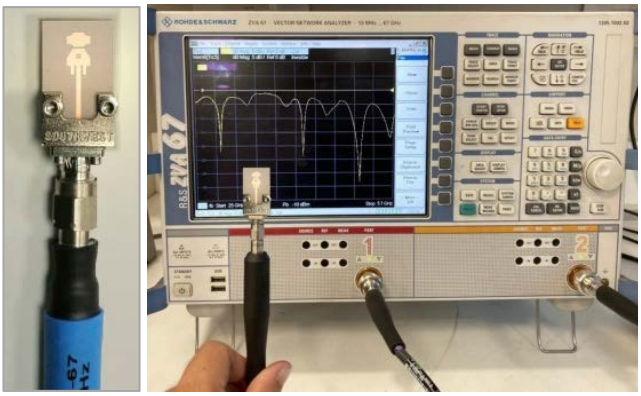

FIGURE 22. Measurement of the reflection coefficient $|S_{11}|$ of the proposed quad-band patch antenna: (a) The fabricated prototype is connected to the end launcher, (b) The antenna is connected to the VNA of Rhode and Schwartz model ZVA67.

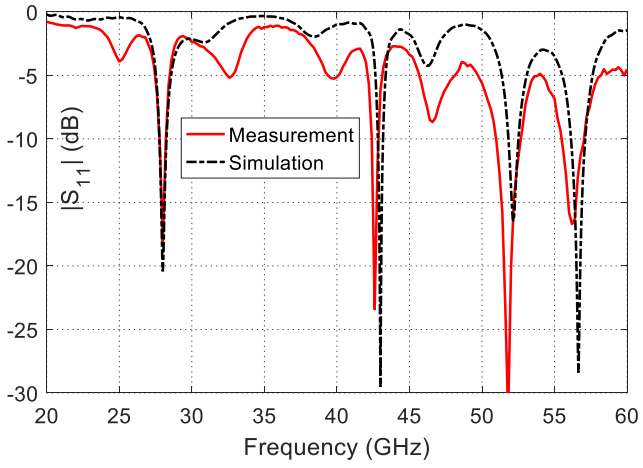

FIGURE 23. Dependence of the reflection coefficient $|S_{11}|$ on the frequency for the patch antenna presented in Fig. 15.

the reference horn antenna A-Info LB018400 and at 43 GHz using the reference horn antenna A-Info LB-12-10-A. The radiation patterns at 52 and 57 GHz are measured using the VNA-ZA67 and the reference horn antenna A-Info LB-12-10-A.

1) MEASUREMENT OF THE ANTENNA IMPEDANCE AND RETURN LOSS

As shown in Fig. 22b, the VNA-ZA67 is used for measuring the frequency response of the reflection coefficient magnitude S_{11}. The frequency dependence of $|S_{11}|$ is presented in Fig. 23. It is shown that the experimental measurements come in good agreement with the simulation results. It is clear that the antenna has good impedance matching at the four frequencies 28, 43, 52, and 57 GHz.

2) MEASUREMENT OF THE ANTENNA RADIATION PATTERNS

One of the experimental setups that are constructed for measuring the radiation patterns of the proposed antenna is shown

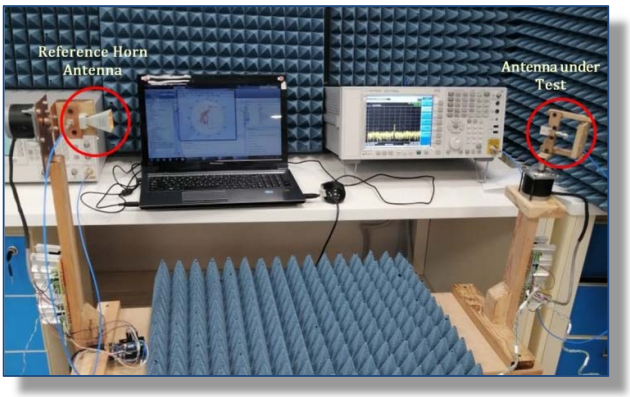

FIGURE 24. Experimental setup for measuring the radiation pattern and gain of the quad-band antenna.

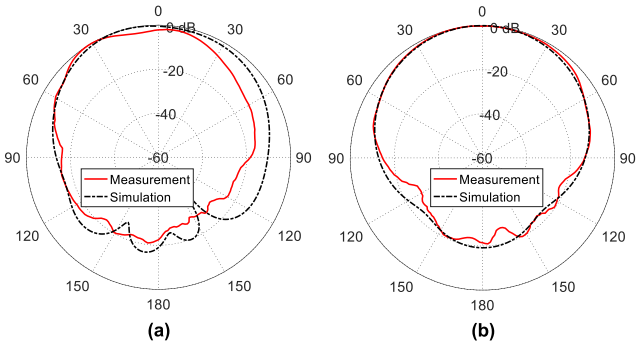

FIGURE 25. Radiation patterns of the proposed quad-band patch antenna at 28 GHz in the elevation planes (a) $\phi = 0°$ and (b) $\phi = 90°$.

in Fig. 24. This setup is employed to measure the elevation radiation patterns at 28 and 43 GHz using the VSG-E8267D and the VSA-N9010A with the A-Info reference-gain horn antennas models LB-018400 for 28 GHz and LB-12-10-A for 43 GHz. A similar experimental setup is constructed to measure the radiation patterns at 52 and 57 GHz using the VNA-ZVA67 with the A-Info reference-gain horn antenna model LB-12-10-A.

The elevation radiation patterns in the planes $\phi = 0°$ and $\phi = 90°$ at the four frequencies 28, 43, 52, and 57 GHz are presented in Fig. 25, 26, 27, and 28, respectively. The experimental measurements show good agreement with the simulation results at all the operational frequencies of the proposed antenna.

3) VERTICALLY AND HORIZONTALLY POLARIZED FIELDS

The vertically and horizontally polarized far field patterns produced by the proposed antenna are presented in Fig. 29. The experimental measurements come in good agreement with the simulation results. As the radiated electric field is mainly parallel to the xz-plane, the radiation in the plane $\phi = 0°$ is dominated by vertical polarization while in the $\phi = 90°$ the radiated fields have both vertically and horizontally polarized components.

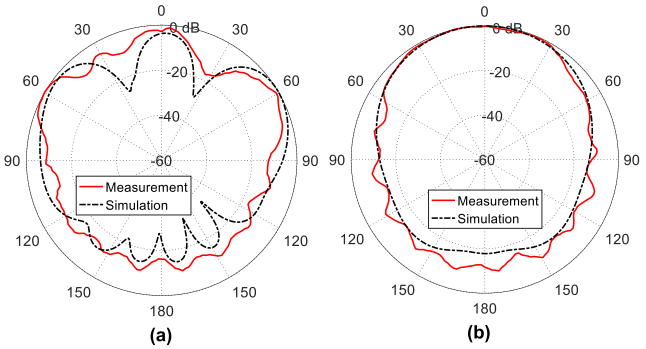

FIGURE 26. Radiation patterns of the proposed quad-band patch antenna at 43 GHz in the elevation planes (a) $\phi = 0°$ and (b) $\phi = 90°$.

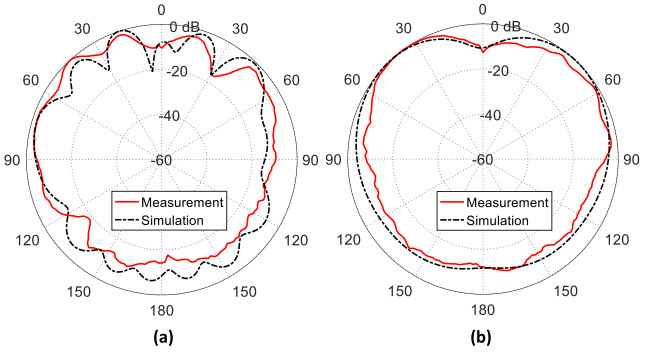

FIGURE 27. Radiation patterns of the proposed quad-band patch antenna at 52 GHz in the elevation planes (a) $\phi = 0°$ and (b) $\phi = 90°$.

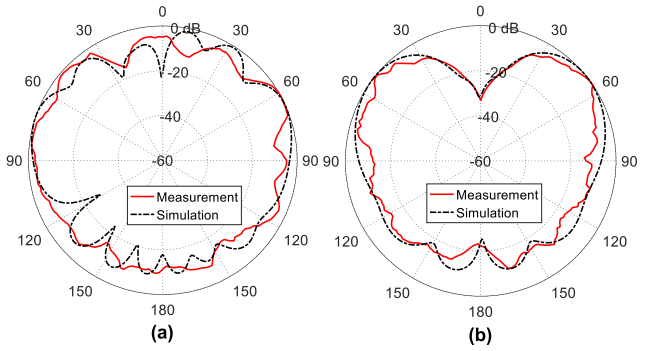

FIGURE 28. Radiation patterns of the proposed quad-band patch antenna at 57 GHz in the elevation planes (a) $\phi = 0°$ and (b) $\phi = 90°$.

4) MEASUREMENT OF THE GAIN AND RADIATION EFFICIENCY

The dependencies of the gain and radiation efficiency of the proposed antenna, presented in Fig. 20, on the frequency are shown in Figs. 30 – 33 over the four operational frequency bands. The experimental results show good agreement with the simulation results for both the maximum gain and radiation efficiency over all the operational frequency bands. It is shown that the maximum gain ranges from 7 to 8 dBi whereas the radiation efficiency ranges from 86% to 90%.

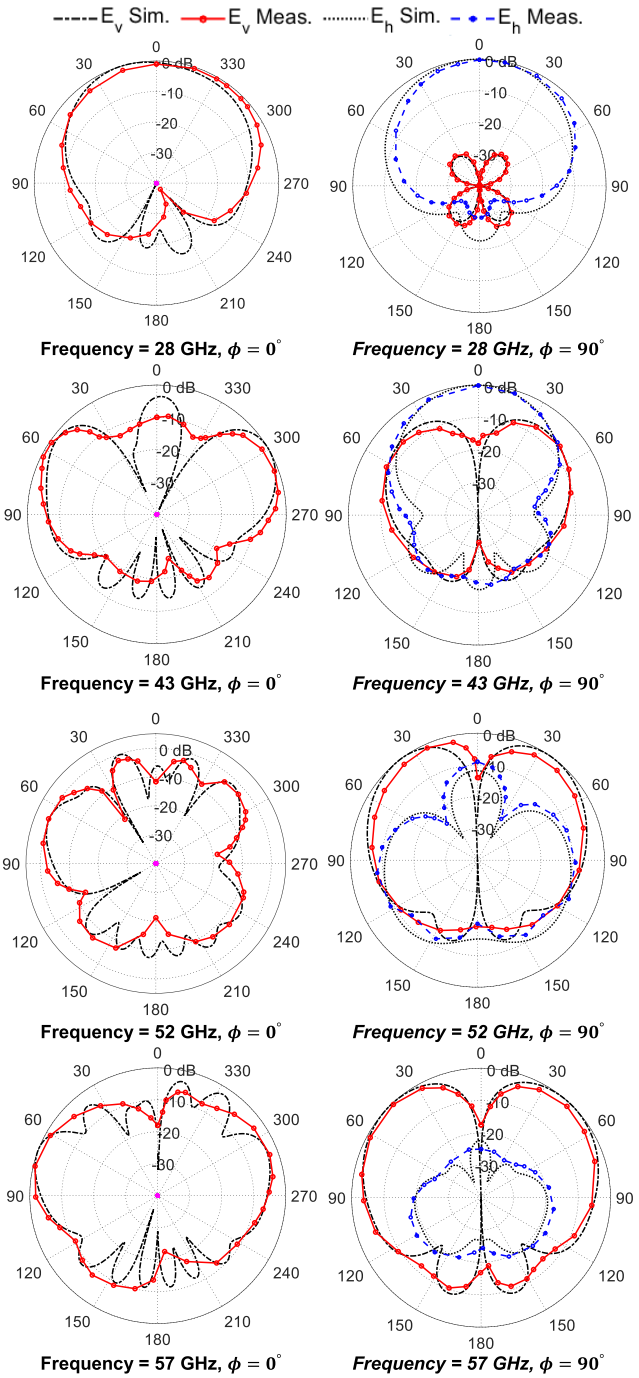

FIGURE 29. Co- and cross-polarized fields at the four operating frequencies.

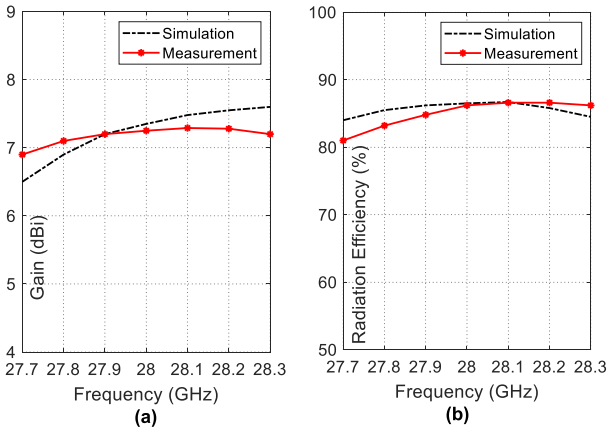

FIGURE 30. Variation of (a) maximum gain and (b) radiation efficiency with the frequency over the first operational frequency band (27.7 – 28.3 GHz).

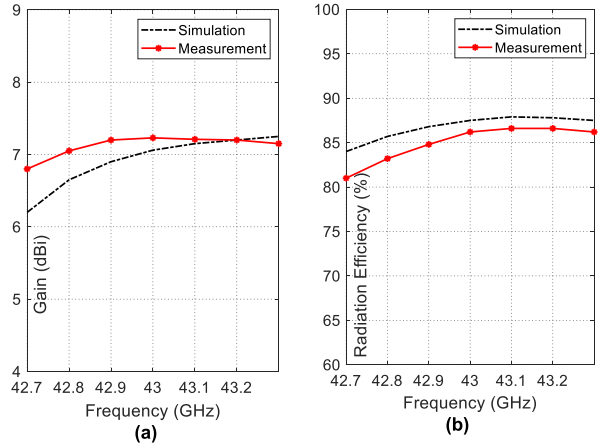

FIGURE 31. Variation of (a) maximum gain and (b) radiation efficiency with the frequency over the second operational frequency band (42.7 – 43.3 GHz).

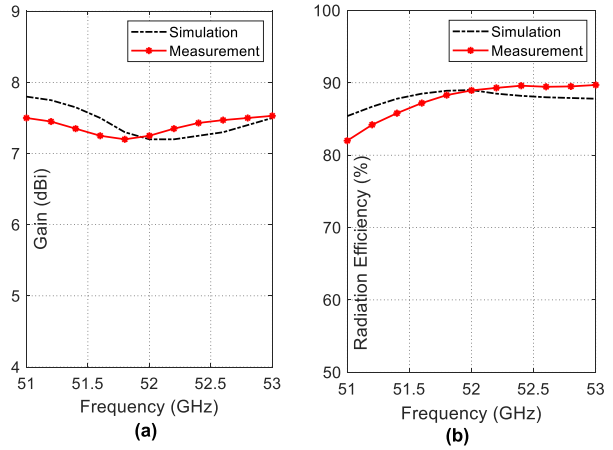

FIGURE 32. Variation of (a) maximum gain and (b) radiation efficiency with the frequency over the third operational frequency band (51.2 – 53.0 GHz).

B. SUMMARY OF THE PROPOSED ANTENNA PERFORMANCE

This section is concerned with providing a summary of the most important performance metrics for the quad-band patch antenna proposed in the present work whose design is presented in Fig. 20. Table 6 gives a summary of the proposed quad-band antenna performance at the four operational frequencies. Table 7 gives comparative performance among some mm-wave patch antennas available in some recent literature and the antenna proposed in the present work.

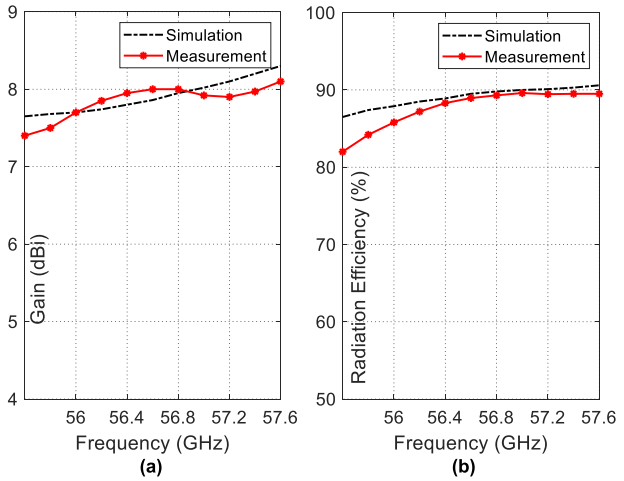

FIGURE 33. Variation of (a) maximum gain and (b) radiation efficiency with the frequency over the fourth operational frequency band (55.7 – 57.5 GHz).

TABLE 6. Achieved frequency bands (obtained experimentally) by the proposed quad-band antenna and the corresponding gain and radiation efficiency.

Center Frequency (GHz)	28	43	52	57
Start Frequency (GHz)	27.7	42.7	51.20	55.7
End Frequency (GHz)	28.3	43.3	53	57.5
Bandwidth (GHz)	0.6	0.6	1.8	1.8
Electric Length (λ)	0.48	0.74	0.91	0.98
BDR	22	53	26	30
Radiation Efficiency (%)	86.5	87.5	89.2	90

TABLE 7. Comparison with other published designs.

Work	[11]	[1]	[10]	[26]	[27]	Present
Center Frequencies (GHz)	28 38	38 45	38 54	23.9 35.5 70.9	28 38 55	28 43 52 57
Gain (dBi)	3.7 5.1	7.6 7.2	6.9 7.4	4.4 3.6 5.6	6.8 7.15 7.4	7.3 7.03 7.2 8.03
Patch Dimensions (mm)	3.7 x 5.1	6 x 6	6.6 x 6	6.19 x 7.25	8 x 8	3.3 x 5.2
Overall Size (mm)	28 X 25	22 X 36	40 X 20	35 X 19	27 X 14	8 X 18
Electric Dimension (λ)	0.6 0.82	0.5 0.75	0.9 0.45	0.7 0.85	0.52 0.64 0.96	0.48 0.74 0.91 0.98
BDR	18 37	30 25	27 22	20 15	25 35 19	22 53 26 30

VI. CONCLUSION

A novel method has been introduced to extend the operation of a microstrip patch antenna that principally radiates at its first-order resonance so as to efficiently radiate over multiple higher-order frequency bands in the mm-wave range. The proposed method relies on modifying the antenna structure by adding some inductively- and capacitively-coupled elements to the primary patch so that it can efficiently radiate at the desired higher frequency bands. It has been explained quantitatively how to use the geometrical parameters of the inductively and capacitively coupled elements for accurate tuning of the multiple resonant frequencies of the antenna. This method has been applied to extend the operation of a primary hexagonal patch antenna (that radiates at 28 GHz as its first-order resonance) so as to operate at additional higher frequency bands around 43, 52, and 57 GHz. Furthermore, and alternative design has been provided for a quad-band printed antenna of composite patch structure that operates efficiently at the mm-wave frequencies 28, 43, 52, and 57 GHz. The corresponding frequency bands are, respectively, (27.7 – 28.3 GHz), (42.7 – 43.3 GHz), (50.2 – 53.0 GHz), and (55.7 – 57.5 GHz). The dimensions of the area occupied by the primary patch and the parasitic elements are 5.2×3.3 mm^2. The achieved antenna gains at each resonant frequency are 7.3, 7.0, 7.2, and 8.0, respectively. It has been shown that the proposed antennas have excellent impedance matching, acceptable radiation patterns, and satisfactory values of the antenna gain. Prototypes have been fabricated for experimental assessment of the proposed antennas including the impedance matching and radiation patterns. The experimental measurements have been shown to agree with the simulation results over all the four operational mm-wave frequency bands.

REFERENCES

[1] R. A. Bhatti, J. H. Choi, and S. O. Park, "Quad-band MIMO antenna array for portable wireless communications terminals," *IEEE Antennas Wireless Propag. Lett.*, vol. 8, pp. 129–132, 2009.
[2] H. S. Wong, S. Kibria, M. T. Islam, J. S. Mandeep, and N. Misran, "Quad band handset antenna for LTE MIMO and WLAN application," *Int. J. Antennas Propag.*, vol. 2014, pp. 1–7, Apr. 2014.
[3] M. Mishra and R. S. Kshetrimayum, "Compact quad-band MIMO antenna array with low mutual coupling for mobile terminal," in *Proc. IEEE Region 10 Symp. (TENSYMP)*, Jun. 2019, pp. 665–670.
[4] C. Rajagopal, N. Noorullakhan, S. B. Suseela, and R. Sankararajan, "Compact modified circular patch quad-band MIMO antenna with high isolation and low correlation," *Int. J. Microw. Wireless Technol.*, vol. 9, no. 3, pp. 581–590, Apr. 2017.
[5] C. şeker, T. Ozturk, and M. Güneşer, "A single band antenna design for future millimeter wave wireless communication at 38 GHz," *Eur. J. Eng. Formal Sci.*, vol. 2, no. 2, pp. 35–39, 2018.
[6] E. M. A. Eldesouki, K. F. A. Hussein, and A. M. El-Nadi, "Circularly polarized arrays of cavity backed slot antennas for X-band satellite communications," *Prog. Electromagn. Res. B*, vol. 9, pp. 179–198, 2008.
[7] K. F. A. Hussein, "Conical linear spiral antenna for tracking, telemetry and command of low Earth orbit satellites," *Prog. Electromagn. Res. C*, vol. 29, pp. 97–107, 2012.
[8] O. A. Elkady, S. A. Abolkassem, A. H. Elsayed, W. A. Hussein, and K. F. A. Hussein, "Microwave absorbing efficiency of Al matrix composite reinforced with nano-Ni/SiC particles," *Results Phys.*, vol. 12, pp. 687–700, Mar. 2019.
[9] M. I. Khattak, A. Sohail, U. Khan, Z. Barki, and G. Witjaksono, "Elliptical slot circular patch antenna array with dual band behaviour for future 5G mobile communication networks," *Prog. Electromagn. Res. C*, vol. 89, pp. 133–147, 2019.
[10] D. Imran, M. M. Farooqi, M. I. Khattak, Z. Ullah, M. I. Khan, M. A. Khattak, and H. Dar, "Millimeter wave microstrip patch antenna for 5G mobile communication," in *Proc. Int. Conf. Eng. Emerg. Technol. (ICEET)*, Feb. 2018, pp. 1–6.

[11] A. A. R. Saad and H. A. Mohamed, "Printed millimeter-wave MIMO-based slot antenna arrays for 5G networks," *AEU-Int. J. Electron. Commun.*, vol. 99, pp. 59–69, Feb. 2019.
[12] H. Santos, P. Pinho, and H. Salgado, "Patch antenna-in-package for 5G communications with dual polarization and high isolation," *Electronics*, vol. 9, no. 8, pp. 12–23, 2020.
[13] A. Farahat and K. Hussein, "Dual-band (28/38 GHz) MIMO antenna system for 5G mobile communications with efficient DoA estimation algorithm in noisy channels," *Appl. Comput. Electromagn. Soc.*, vol. 36, no. 3, pp. 282–294, Apr. 2021.
[14] A. E. Farahat and K. F. A. Hussein, "28/38 GHZ dual-band Yagi-Uda antenna with corrugated radiator and enhanced reflectors for 5G MIMO antenna systems," *Prog. Electromagn. Res. C*, vol. 101, pp. 159–172, 2020.
[15] M. AboEl-Hassan, A. E. Farahat, and K. F. Hussein, "Compact-size quad-band patch antenna for 5G mobile communications," *Microw. Opt. Technol. Lett.*, vol. 63, no. 12, pp. 3067–3071, Dec. 2021.
[16] E. S. Ahmed, "Multiband CPW-fed rectangular ring microstrip antenna design for wireless communications," in *Proc. IEEE Jordan Conf. Appl. Electr. Eng. Comput. Technol. (AEECT)*, Dec. 2011, pp. 1–5.
[17] A. Gupta and P. Chawla, "Fractal: Impact of feeding techniques on the radiation pattern of modified star triangular fractal," in *Proc. 1st Int. Conf. Next Gener. Comput. Technol. (NGCT)*, Sep. 2015, pp. 441–446.
[18] A. D. Boursianis, M. S. Papadopoulou, J. Pierezan, V. C. Mariani, L. S. Coelho, P. Sarigiannidis, S. Koulouridis, and S. K. Goudos, "Multi-band patch antenna design using nature-inspired optimization method," *IEEE Open J. Antennas Propag.*, vol. 2, pp. 151–162, 2020.
[19] P. S. Bakariya, S. Dwari, M. Sarkar, and M. K. Mandal, "Proximity-coupled multiband microstrip antenna for wireless applications," *IEEE Antennas Wireless Propag. Lett.*, vol. 14, pp. 646–649, 2014.
[20] J. Kim, T. Jung, H. Ryu, J. Woo, C. Eun, and D. K. Lee, "Compact multiband microstrip antenna using inverted-L- and T-shaped parasitic elements," *IEEE Antennas Wireless Propag. Lett.*, vol. 12, pp. 1299–1302, 2013.
[21] Z. Hasan, A. Zaman, and A. Ahmed, "Design and fabrication of a circular microstrip patch antenna for GPS application," *Int. J. Electron. Commun. Technol. (IJECT)*, vol. 8, no. 3, pp. 54–57, Jul./Sep. 2017.
[22] M. Z. Rahman, K. C. D. Nath, and M. Mynuddin, "Performance analysis of an inset-fed circular microstrip patch antenna using different substrates by varying notch width for wireless communications," *Int. J. Electromagn. Appl.*, vol. 10, no. 1, pp. 19–29, Jan. 2020.
[23] M. R. M. Shah, M. A. A. Aziz, M. K. Suaidi, and M. A. Rahim, "Dual linearly polarized microstrip array antenna," in *Trends in Telecommunications Technologies*. U.K.: IntechOpen, 2010.
[24] M. A. Matin and A. I. Sayeed, "A design rule for inset-fed rectangular microstrip patch antenna," *WSEAS Trans. Commun.*, vol. 9, no. 1, pp. 63–72, 2010.
[25] M. A. El-Hassan, A. E. Farahat, and K. F. A. Hussein, "Quad-band patch antenna for future generations of mobile handsets," in *Proc. 9th Int. Japan-Africa Conf. Electron., Commun., Computations (JAC-ECC)*, Dec. 2021, pp. 34–38.
[26] S. Punith, S. K. Praveenkumar, A. A. Jugale, and M. R. Ahmed, "A novel multiband microstrip patch antenna for 5G communicationsm," in *Proc. 3rd Int. Conf. Comput. Netw. Commun.*, 2020, pp. 2080–2086.
[27] M. Hussain, S. M. R. Jarchavi, S. I. Naqvi, U. Gulzar, S. Khan, M. Alibakhshikenari, and I. Huynen, "Design and fabrication of a printed tri-band antenna for 5G applications operating across Ka-, and V-band spectrums," *Electronics*, vol. 10, no. 21, p. 2674, Oct. 2021.

ASMAA E. FARAHAT received the B.Sc. and M.Sc. degrees from the Department of Biomedical Engineering, Faculty of Engineering, Cairo University, in 2002 and 2006, respectively, and the Ph.D. degree from Ain Shams University, in 2012. She is currently an Associate Professor with the Department of Microwave Engineering, Electronics Research Institute. She has work experience in scientific research for about 17 years. She has published more than 30 papers in international, regional and local scientific journals, and conferences. She has worked as a secondary investigator for three research projects. Her research interests include antennas, electromagnetic wave propagation, risk assessment of human exposure to microwave radiation, remote sensing systems, and radar systems.

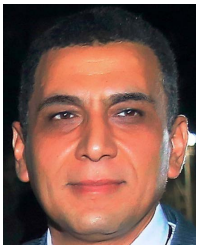

KHALID F. A. HUSSEIN received the B.Sc., M.Sc., and Ph.D. degrees from the Department of Electronics and Electrical Communications, Faculty of Engineering, Cairo University, in 1990, 1995, and 2001, respectively. He has served as the Head of the Microwave Engineering Department, Electronics Research Institute for up to four years. He is currently a Professor at the Department of Microwave Engineering, Electronics Research Institute. He has work experience in scientific research for more than 29 years. He has teaching experience in engineering colleges in many universities for more than 20 years. He has supervised more than 70 doctoral and master's degree theses. He has worked as a principal investigator for four research projects and the Head of the research group in four other research projects. He has designed and implemented several satellite antennas between prototypes and finished products. He has provided scientific consultations and conducted field measurements related to the design and distribution of mobile communication base station antennas for good signal coverage in behalf of many Egyptian and international companies. He has published more than 100 papers in international, regional and local scientific journals, and conferences. His research interests include antennas, electromagnetic wave propagation, risk assessment of human exposure to microwave radiation, optical communications, photonics, quantum computing, radar systems, particularly ground penetrating radar (GPR), synthetic aperture radar (SAR), and remote sensing systems. He has been a member of the Egyptian Space Program (currently the Egyptian Space Agency) for more than eight years.

MAY ABO. EL-HASSAN received the B.Sc. and M.Sc. degrees in communications and electronic engineering and communications engineering from Menoufia University, Egypt, in 2007 and 2014, respectively, and the Ph.D. degree, in 2020. She is currently a Researcher with the Department of Microwave Engineering, Electronics Research Institute. She has published more than 18 papers in international, regional and local scientific journals, and conferences. Her current research interests include RFID, areas in antennas, chip-less tags, SAR, and beam shaping.